Geochemistry Geophysics Geosystems G3
AN ELECTRONIC JOURNAL OF THE EARTH SCIENCES
Published by AGU and the Geochemical Society

Article
Volume 10, Number 4
2 April 2009
Q04004, doi:10.1029/2008GC002331
ISSN: 1525-2027

Geochemical characteristics of the Miocene eolian deposits in China: Their provenance and climate implications

Meiyan Liang
Key Laboratory of Cenozoic Geology and Environment, Institute of Geology and Geophysics, Chinese Academy of Sciences, P.O. Box 9825, Beijing 100029, China

Also at College of Earth Sciences, Graduate University of the Chinese Academy of Sciences, Beijing 100049, China

Zhengtang Guo
Key Laboratory of Cenozoic Geology and Environment, Institute of Geology and Geophysics, Chinese Academy of Sciences, P.O. Box 9825, Beijing 100029, China (ztguo@mail.iggcas.ac.cn)

A. Julia Kahmann
Department of Geology, Baylor University, One Bear Place 97354, Waco, Texas 76798-7354, USA

Frank Oldfield
Department of Geography, University of Liverpool, Liverpool L69 7ZT, UK

[1] In the Loess Plateau in northern China, the Quaternary loess-soil sequences, the Hipparion Red Earth of eolian origin (Red Clay), and the Miocene loess-soil sequences constitute a near-continuous terrestrial record of paleoclimates for the past 22 Ma. In this study, Miocene loess and paleosol samples from Qinan (QA-I) were analyzed for their major, trace, and rare earth element chemistry and compared with the Plio-Pleistocene samples from Xifeng with emphasis on their provenance and paleoclimatic implications. The results show similar geochemical signatures for the eolian deposits of different ages, and they are also comparable to the average composition of the upper continental crust. These suggest that the dust materials were all derived from well-mixed sedimentary protoliths which had undergone numerous upper crustal recycling processes. They also support the notion of broadly similar source areas and dust-transporting trajectories for different periods since the early Neogene. The slightly higher K_2O, Fe_2O_3, and MgO concentrations and loss on ignition values and the lower Na_2O content in the Miocene loess samples compared to their Quaternary counterparts are attributable to the finer grain size of the Miocene loess associated with weaker dust-carrying winds. In comparison with some loess in Europe and America with less extensive sources, eolian deposits from northern China show higher Cs and lower Zr and Hf content. This is attributable to the sorting processes from remoter sources during transportation and could be regarded as an indication of the desert origin of the loess deposits. Miocene paleosol samples show higher chemical index of alteration values and lower CaO, MgO, and Na_2O concentrations than does the intervening loess, indicating stronger weathering of the paleosols. However, the moderate chemical weathering of the paleosol samples indicates a constant semiarid and subhumid climatic range in northern China since the early Miocene.

Components: 9791 words, 8 figures, 3 tables.

Keywords: geochemistry; Miocene loess-soil sequence; paleoclimate; Asian monsoon.

Index Terms: 1065 Geochemistry: Major and trace element geochemistry; 3344 Atmospheric Processes: Paleoclimatology (0473, 4900); 1020 Geochemistry: Composition of the continental crust.

Received 19 November 2008; **Revised** 10 February 2009; **Accepted** 22 February 2009; **Published** 2 April 2009.

Liang, M., Z. Guo, A. J. Kahmann, and F. Oldfield (2009), Geochemical characteristics of the Miocene eolian deposits in China: Their provenance and climate implications, *Geochem. Geophys. Geosyst.*, *10*, Q04004, doi:10.1029/2008GC002331.

1. Introduction

[2] A combination of the Quaternary loess-soil sequences [*Liu*, 1985; *Wen*, 1989; *Kukla et al.*, 1990], the late Miocene-Pliocene Red Earth formation of eolian origin [*Ding et al.*, 1998a; *Sun et al.*, 1998; *An et al.*, 2001; *Guo et al.*, 2001] and the Miocene loess-soil sequences [*Guo et al.*, 2002; *Liu et al.*, 2005, 2006; *Hao and Guo*, 2007] in the Loess Plateau in northern China provides a near-complete record of the Asian monsoon climate and inland aridification for the past 22 Ma. The eolian origin of the Miocene sequences has already been demonstrated by sedimentological, pedological and preliminary geochemical characteristics [*Guo et al.*, 2002], terrestrial fossil evidence [*Li et al.*, 2006, 2008] and the spatial correlativity of stratigraphy and magnetic susceptibility over long distance [*Liu et al.*, 2005; *Hao and Guo*, 2007; *Guo et al.*, 2008]. They indicate that sizable deserts in the Asian interior and the Asian monsoon system had already developed by 22 Ma. Meanwhile, the alternations between loess and paleosol layers indicate cyclical changes of summer and winter monsoons [*Guo et al.*, 2002].

[3] The geochemical characteristics of the Quaternary loess deposits [*Liu*, 1985; *Wen*, 1989; *Gallet et al.*, 1996, 1998; *Chen et al.*, 1998, 2001; *Gu et al.*, 2000] and the eolian Red Earth [*Ding et al.*, 1998b, 2001; *Gu et al.*, 1999; *Guo et al.*, 2001] have been well documented and provided a significant amount of information about their origin, source provenance and paleoclimate conditions. In contrast, little is known about the Miocene loess-soil sequences beyond preliminary reports [*Guo et al.*, 2002].

[4] This study aims to (1) characterize the major, trace and rare earth elemental (REE) geochemistry of the Miocene loess and paleosol samples from QA-I [*Guo et al.*, 2002] and compare these with the well-known Plio-Pleistocene eolian sequence at Xifeng [*Kukla et al.*, 1990; *Sun et al.*, 1998; *Guo et al.*, 2004]; (2) interpret the implications of the eolian deposits of different ages in terms of dust sources and atmospheric circulation; and (3) compare the chemical weathering characteristics of these eolian deposits and discuss their paleoclimate significance.

2. Sampling and Experimental Methods

[5] The QA-I (105°27′ E, 35°02′ N) Miocene loess-soil section, spanning the interval from 22 to 6.2 Ma, is 253.1 m thick and is located in Qinan county (Gansu Province of China) (Figure 1). It contains more than 230 visually definable reddish paleosol layers interbedded with yellow-brown or brown loess layers [*Guo et al.*, 2002]. To ensure a good temporal coverage, sixty samples (30 from loess and 30 from paleosol layers), as equally spaced as possible, were selected along the QA-I section for major element analysis, among which twelve samples were selected for trace element analysis. Because of the general lack of Plio-Pleistocene eolian sections at the same locality, thirty samples from the Quaternary (15 from loess and 15 from paleosol layers) and six samples from the late Miocene-Pliocene Red Earth at Xifeng (3 from loess and 3 from paleosol layers) were selected for major and trace elemental analyses. The total thickness of the Xifeng section is 228.8 m. The distributions of the samples along the studied sections are given in Tables 1–3.

[6] After the eolian dust was deposited, varying degrees of decalcification during pedogenesis caused the calcium carbonate content to vary. To remove the influence of carbonate translocation, all the samples were leached of calcium carbonate using 1mol/l acetic acid (HAc) as this method is thought to leach totally the carbonate fraction without significant effect on silicates or iron oxides [*Chen et al.*, 1996; *Liu et al.*, 2002]. Our test experiment on thirty samples (Figure 2) also reveals only small differences for pretreated and posttreated samples with the exception of CaO and MnO. The significant change in MnO was also noted in earlier studies [*Ji and Chen*, 2000; *Liu et al.*, 2002] and is attributable to the removal of Mn^{2+} residing in carbonate during carbonate leaching.

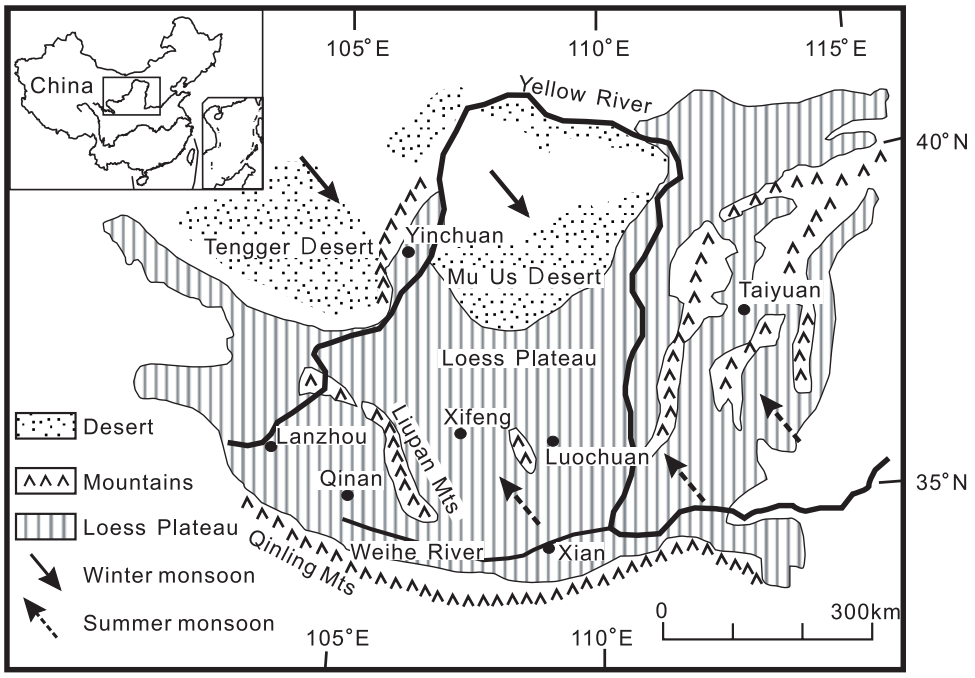

Figure 1. Map showing the Loess Plateau, the locations of the sites referred to, and the east Asian summer and winter monsoons. The area covered is shown by the rectangular within the map of China (top left inset).

[7] Before acid dissolution, all samples were finely ground using an agate mortar. Major element abundances were determined using a Shimadzu XRF-1500 spectrometer in the Institute of Geology and Geophysics, Chinese Academy of Sciences (IGG-CAS). All major element percentages are converted to oxide percentages. Analytical uncertainties are ±2% for all major elements except for P_2O_5 and MnO (up to ±10%). Loss on ignition (LOI) was obtained by weighing after 1 h of heating at 950°C.

[8] The trace element compositions were determined using an ICP-MS (ELEMENT, Finnigan MAT) at IGG-CAS. The analytical uncertainties were less than 10% for most of the trace elements. To ensure refractory mineral dissolution, samples were dissolved using a two-step procedure as reported in the work of *Gallet et al.* [1996]. The combined water was also analyzed for chemical research and was determined by Penfield gravimetry [*Penfield*, 1894].

3. Results and Discussion

3.1. Major Element Characteristics

[9] Major element data and their average content for Miocene samples are given in Table 1; the Plio-Pleistocene samples are also given for comparison. Upper continental crust (UCC)-normalized abundances for the loess and paleosol samples of different ages are shown in Figure 3. The data for the Plio-Pleistocene samples are in good agreement with earlier results [*Liu*, 1985; *Wen*, 1989; *Gallet et al.*, 1996, 1998; *Ding et al.*, 1997, 2001; *Gu et al.*, 1999, 2000; *Chen et al.*, 2001; *Guo et al.*, 2001]. The major elemental composition of the Miocene loess is dominated by SiO_2, Al_2O_3, Fe_2O_3, MgO and K_2O. This is similar to the Pleistocene and Pliocene loess samples, and also resembles that of the average of UCC [*Taylor and McLennan*, 1985; *McLennan*, 2001].

[10] Nevertheless, all the loess samples of different ages from China show a slightly higher TiO_2, Fe_2O_3, MgO and lower Na_2O, CaO compared to UCC (Figure 4a). In comparison with the younger eolian deposits (Figure 4a), the Miocene loess samples show slightly lower SiO_2 and Na_2O content, higher Al_2O_3, Fe_2O_3 and K_2O content. Combined water and LOI content are also higher than in the Plio-Pleistocene samples (Table 1).

[11] The plot of Na_2O/Al_2O_3 versus K_2O/Al_2O_3 was introduced by *Garrels and Mackenzie* [1971] to reflect the removal of Na versus K during the alternation of igneous to sedimentary rocks as Na is removed and K is retained in shales. These plots for eolian samples are closely similar to each other, but all show a clear Na depletion in comparison

Table 1. Major Element Concentrations of Eolian Sediments From Different Ages[a]

Depth (m)	Sample	SiO_2	TiO_2	Al_2O_3	Fe_2O_3	MnO	MgO	CaO	Na_2O	K_2O	P_2O_5	Total	CIA	LOI	Combined Water
							Qinan Miocene Loess								
4.10	20GJ41	66.04	0.84	17.27	7.03	0.12	3.18	1.09	1.06	3.22	0.15	100	70.51	6.01	
10.80	20GJ108	65.50	0.87	16.80	7.07	0.10	3.22	1.83	1.13	3.36	0.11	100	65.49	7.05	4.92
22.80	20GJ228	65.30	0.86	17.35	7.29	0.13	3.41	1.05	1.12	3.33	0.16	100	70.16	5.61	
29.60	20GJ296	64.96	0.87	17.30	7.20	0.14	3.45	1.29	1.28	3.29	0.22	100	68.32	6.38	
36.40	20GJ364	65.49	0.89	17.18	7.31	0.13	3.34	0.93	1.09	3.47	0.15	100	70.26	7.00	4.71
38.64	20GJ383	65.13	0.84	17.30	7.15	0.15	3.36	1.13	1.37	3.38	0.18	100	68.42	6.77	
48.20	20ZW65	65.44	0.85	17.32	7.10	0.12	3.60	1.17	1.09	3.13	0.18	100	70.27	6.63	
60.90	20ZW192	65.86	0.87	17.30	6.99	0.13	3.23	1.18	1.16	3.16	0.13	100	69.79	6.00	
66.60	20ZW249	65.86	0.89	16.86	7.06	0.12	3.14	1.41	1.09	3.38	0.19	100	67.77	7.01	5.55
77.70	20ZW390	65.53	0.85	17.38	7.16	0.15	3.31	0.86	1.33	3.29	0.13	100	70.34	5.61	
81.40	20ZW427	66.94	0.83	16.21	6.54	0.10	3.28	1.38	1.41	3.08	0.22	100	66.46	5.38	
97.70	20ZW590	65.61	0.85	17.20	7.21	0.14	3.21	1.10	1.30	3.28	0.12	100	69.11	6.69	4.35
105.90	99QW1092	67.12	0.82	16.37	6.66	0.11	3.19	0.93	1.49	3.16	0.15	100	68.39	5.46	
109.60	99QW1129	67.16	0.82	16.29	6.60	0.11	3.18	0.97	1.53	3.18	0.16	100	67.81	5.60	
116.40	20QW108	67.15	0.81	16.30	6.57	0.11	3.20	1.03	1.61	3.03	0.20	100	67.60	5.38	
121.80	20QW162	68.30	0.84	15.57	6.16	0.07	3.16	1.27	1.44	2.99	0.20	100	66.31	5.45	
132.30	20QW271	67.87	0.79	16.07	6.16	0.12	3.17	1.12	1.62	2.91	0.18	100	67.18	5.18	
145.10	99QW1540	66.08	0.85	17.08	7.01	0.11	3.31	0.94	1.20	3.24	0.18	100	70.31	5.43	
148.89	99QW1580	66.18	0.81	16.41	6.65	0.10	3.67	1.61	1.54	3.13	0.22	100	64.94	6.14	
152.74	99QW1622	66.68	0.84	16.95	6.73	0.11	3.13	0.96	1.27	3.14	0.19	100	70.06	5.33	
165.90	99QW1759	66.64	0.80	16.35	6.61	0.10	3.48	1.20	1.55	3.10	0.17	100	66.87	6.06	
195.00	99QW2079	68.57	0.78	15.72	6.00	0.12	3.01	0.82	1.60	3.17	0.21	100	67.54	4.66	
203.50	99QW2164	67.80	0.79	16.23	6.32	0.06	2.92	1.14	1.38	3.13	0.22	100	67.68	5.85	
210.30	99QW2232	69.72	0.75	15.20	5.81	0.07	2.78	0.92	1.47	3.03	0.23	100	67.28	5.30	
218.80	99QW2317	69.23	0.81	15.85	6.20	0.10	2.45	0.87	1.36	2.99	0.13	100	69.14	5.55	
226.86	99QW2398	67.92	0.77	16.02	6.27	0.05	2.98	1.47	1.27	3.01	0.24	100	66.60	6.68	
228.54	99QW2412	67.92	0.77	16.02	6.27	0.05	2.98	1.47	1.27	3.01	0.24	100	66.60	6.68	4.85
234.60	99QW3345	68.14	0.78	15.59	5.94	0.06	3.28	1.56	1.54	2.91	0.21	100	64.65	6.38	
243.50	99QW3434	69.79	0.74	15.38	5.66	0.05	2.77	1.26	1.29	2.86	0.19	100	67.14	5.75	
247.70	99QW3476	68.57	0.80	15.31	5.93	0.05	2.88	1.53	1.56	3.14	0.23	100	63.60	6.20	4.85
	average	66.95	0.82	16.47	6.62	0.10	3.18	1.18	1.35	3.15	0.18		67.89	5.97	4.87
							Qinan Miocene Soil								
0.80	20GJ8	65.95	0.87	16.95	7.07	0.12	3.13	1.24	1.08	3.40	0.20	100	68.67	6.75	4.95
8.40	20GJ84	65.82	0.84	17.28	7.12	0.11	3.24	0.93	1.18	3.35	0.13	100	70.38	5.70	
17.60	20GJ176	65.77	0.89	17.12	7.24	0.13	3.30	0.88	1.07	3.49	0.11	100	70.56	6.51	4.54
25.60	20GJ256	65.51	0.86	17.30	7.26	0.13	3.25	0.97	1.22	3.38	0.13	100	69.94	5.69	
33.60	20GJ336	64.98	0.84	17.59	7.25	0.13	3.46	1.14	1.17	3.29	0.15	100	69.91	6.35	
45.90	20GJ459	65.17	0.84	17.37	7.11	0.14	3.42	1.19	1.24	3.27	0.26	100	69.13	6.57	
50.30	20ZW86	65.92	0.83	17.16	7.08	0.13	3.54	1.08	1.10	3.05	0.11	100	70.74	7.31	
55.20	20ZW135	65.83	0.85	17.27	7.04	0.11	3.34	1.10	1.14	3.17	0.15	100	70.25	6.54	
71.33	20ZW324	65.02	0.87	17.95	7.40	0.13	3.04	1.16	1.07	3.24	0.13	100	70.83	6.01	
80.00	20ZW413	66.40	0.87	16.51	6.87	0.13	3.24	1.15	1.29	3.34	0.20	100	67.84	6.33	5.04
83.50	20ZW448	66.27	0.89	16.96	7.36	0.14	3.19	0.73	1.08	3.31	0.06	100	71.64	7.43	5.22
91.90	20ZW532	65.11	0.84	17.72	7.36	0.14	3.23	1.01	1.27	3.24	0.10	100	70.46	6.78	
101.12	99QW1044	67.40	0.81	16.04	6.51	0.10	3.30	1.28	1.42	3.01	0.14	100	66.88	6.01	
108.30	99QW1116	67.22	0.82	16.27	6.53	0.15	3.18	0.91	1.65	3.12	0.15	100	67.71	5.40	
118.00	20QW124	68.03	0.87	16.35	6.48	0.15	2.90	0.61	1.38	3.15	0.08	100	70.64	5.60	
126.00	20QW204	66.83	0.86	16.38	6.75	0.16	3.34	0.87	1.34	3.35	0.13	100	68.82	6.95	5.46
136.00	99QW1449	66.84	0.82	16.82	6.75	0.09	3.29	0.91	1.19	3.14	0.15	100	70.56	5.23	
140.10	99QW1490	66.31	0.83	16.90	6.80	0.12	3.39	0.96	1.26	3.24	0.20	100	69.75	5.21	
149.07	99QW1582	66.52	0.88	16.74	6.97	0.17	3.17	0.72	1.34	3.39	0.12	100	69.97	6.21	5.10
159.12	99QW1690	66.64	0.87	16.59	6.92	0.20	3.19	0.76	1.45	3.24	0.13	100	69.50	6.12	5.07
166.30	99QW1763	66.65	0.88	16.51	6.94	0.18	3.14	0.79	1.40	3.36	0.14	100	69.05	6.17	4.35
191.90	99QW2048	68.32	0.78	15.70	6.06	0.08	3.01	1.02	1.48	3.25	0.29	100	66.74	4.95	
198.70	99QW2116	67.02	0.75	16.26	6.49	0.07	3.14	0.95	1.60	3.45	0.26	100	66.73	5.95	
206.00	99QW2189	67.21	0.80	16.78	6.65	0.09	2.86	0.94	1.26	3.26	0.15	100	69.60	6.12	
215.00	99QW2279	68.02	0.81	16.37	6.41	0.08	2.66	0.95	1.33	3.16	0.21	100	69.01	5.71	
222.30	99QW2352	68.78	0.84	16.21	6.34	0.13	2.70	0.36	1.47	3.10	0.06	100	71.58	5.96	
231.80	99QW3317	69.00	0.83	15.97	6.17	0.15	2.74	0.43	1.66	2.97	0.07	100	70.33	5.60	

Table 1. (continued)

Depth (m)	Sample	SiO_2	TiO_2	Al_2O_3	Fe_2O_3	MnO	MgO	CaO	Na_2O	K_2O	P_2O_5	Total	CIA	LOI	Combined Water
238.00	99QW3379	68.37	0.84	15.99	6.21	0.14	2.79	0.85	1.51	3.02	0.29	100	68.65	4.75	
251.70	99QW3516	67.43	0.81	16.62	6.41	0.13	2.79	0.92	1.46	3.21	0.22	100	68.73	6.26	
253.10	99QW3530	69.00	0.89	16.54	6.54	0.12	2.50	0.40	1.23	3.36	0.07	100	72.14	6.78	5.19
	average	66.78	0.84	16.74	6.80	0.13	3.11	0.91	1.31	3.24	0.15		69.56	6.10	4.99
							Xifeng Pliocene Loess								
172.10	XFRC49	73.81	0.69	12.93	4.80	0.11	2.19	0.93	1.69	2.77	0.09	100	63.33	4.08	3.02
172.40	XFRC52	67.27	0.84	16.57	6.72	0.11	3.22	0.85	1.17	3.12	0.12	100	70.70	6.15	
183.20	XFRC160	68.27	0.83	15.68	6.32	0.11	3.12	1.00	1.42	3.11	0.15	100	67.54	5.52	4.07
	average	69.78	0.78	15.06	5.95	0.11	2.84	0.93	1.43	3.00	0.12		67.19	5.25	3.55
							Xifeng Pliocene Soil								
174.90	XFRC77	69.83	0.82	14.93	5.89	0.10	2.75	1.06	1.53	2.93	0.16	100	66.20	5.03	3.80
176.30	XFRC91	72.78	0.71	13.99	5.18	0.07	2.39	0.71	1.34	2.73	0.08	100	68.37	4.25	4.17
197.30	XFRC301	68.70	0.85	16.02	6.38	0.09	2.80	0.76	1.30	2.99	0.12	100	70.33	5.30	
	average	70.44	0.79	14.98	5.82	0.09	2.65	0.84	1.39	2.88	0.12		68.30	4.86	3.99
							Xifeng Pleistocene Loess								
8.50	XFC85	69.59	0.78	14.94	5.63	0.09	2.68	1.35	1.97	2.78	0.19	100	63.11	4.63	
18.90	XFC189	70.44	0.79	14.36	5.34	0.08	2.64	1.60	1.94	2.66	0.15	100	61.48	3.66	
29.90	XFC339	70.90	0.71	14.05	5.44	0.08	2.57	1.42	1.98	2.67	0.17	100	61.66	3.62	
39.80	XF1213	69.78	0.80	14.59	5.76	0.10	2.70	1.19	1.99	2.93	0.17	100	62.86	4.21	3.39
45.30	XF1267	70.47	0.82	14.63	5.76	0.10	2.39	1.04	1.76	2.88	0.13	100	64.88	4.60	3.50
61.00	XF762	70.34	0.76	14.56	5.48	0.08	2.65	1.33	1.84	2.78	0.18	100	63.22	4.51	
71.80	XF870	69.74	0.74	15.06	5.70	0.09	2.65	1.23	1.81	2.79	0.18	100	64.58	4.93	
83.60	XF962	69.83	0.77	14.98	5.70	0.09	2.65	1.20	1.74	2.86	0.18	100	64.76	4.55	
96.10	XF1113	69.66	0.73	14.72	5.53	0.08	2.70	1.80	1.82	2.77	0.19	100	61.31	4.55	
98.30	XF1135	69.22	0.76	15.54	6.01	0.12	2.50	1.04	1.71	2.97	0.14	100	66.20	4.65	
104.10	XF46	70.57	0.72	14.76	5.48	0.08	2.59	1.17	1.73	2.73	0.16	100	65.03	4.38	
110.90	XF114	69.88	0.77	14.84	5.58	0.08	2.77	1.48	1.79	2.66	0.14	100	63.52	4.07	
125.20	98XF127	71.04	0.76	14.62	5.47	0.09	2.46	1.01	1.64	2.77	0.15	100	66.02	3.58	
138.20	XF300	68.69	0.78	15.98	6.13	0.11	2.76	0.89	1.54	2.99	0.13	100	68.36	5.32	
143.30	XF351	71.09	0.72	14.73	5.54	0.09	2.41	0.95	1.60	2.72	0.15	100	66.83	4.58	
	average	70.08	0.76	14.82	5.64	0.09	2.61	1.25	1.79	2.80	0.16		64.26	4.39	3.45
							Xifeng Pleistocene Soil								
14.90	XFC149	70.24	0.82	15.17	5.85	0.10	2.31	0.85	1.78	2.76	0.12	100	67.02	5.43	
26.70	XFC267	69.77	0.76	14.87	5.67	0.09	2.61	1.41	1.84	2.80	0.16	100	63.23	4.51	
34.60	XF1161	69.73	0.77	15.02	5.81	0.11	2.70	1.18	1.79	2.75	0.14	100	65.04	4.47	
41.10	XF1226	69.15	0.78	15.37	6.23	0.11	2.57	0.98	1.75	2.94	0.12	100	66.19	4.71	3.87
50.60	XF1313	68.62	0.78	15.98	6.53	0.12	2.63	0.66	1.63	2.97	0.09	100	69.22	5.31	
64.70	XF799	69.35	0.75	15.39	5.91	0.11	2.59	1.15	1.71	2.88	0.16	100	65.69	4.82	
73.90	XF891	69.95	0.73	14.90	5.61	0.10	2.67	1.25	1.88	2.75	0.17	100	64.08	4.90	
85.90	XF1011	68.86	0.76	15.66	6.03	0.11	2.63	1.09	1.75	2.98	0.15	100	65.93	4.80	
94.70	XF1099	69.11	0.80	15.52	6.11	0.11	2.56	1.00	1.57	3.07	0.15	100	66.75	5.21	
100.70	XF12	69.14	0.81	15.45	6.02	0.10	2.63	0.99	1.68	3.03	0.15	100	66.30	4.80	
105.90	XF64	71.75	0.75	14.35	5.38	0.09	2.30	0.96	1.51	2.80	0.11	100	66.39	3.48	
112.90	XF134	69.04	0.82	15.62	6.12	0.11	2.64	1.00	1.45	3.04	0.15	100	67.53	3.88	
128.00	XF198	69.46	0.80	15.39	5.99	0.10	2.67	0.98	1.50	2.96	0.15	100	67.31	4.92	
140.00	XF318	69.56	0.76	15.48	5.86	0.09	2.70	0.92	1.63	2.85	0.15	100	67.53	4.95	
146.40	XF382	71.56	0.74	14.49	5.39	0.08	2.41	0.95	1.52	2.73	0.14	100	66.88	4.57	
	average	69.69	0.77	15.24	5.90	0.10	2.57	1.02	1.67	2.89	0.14		66.34	4.72	3.87
	UCC[b]	66.00	0.68	15.20	5.00	0.07	2.20	4.20	3.90	3.40		100			

[a] In wt %, recalculated on a volatile-free basis.
[b] *Taylor and McLennan* [1985] and *McLennan* [2001].

Table 2. Trace Element Concentrations of Eolian Sediments From Different Ages[a]

Depth (m)	Sample	Li	Be	Sc	Co	Ni	Ga	Rb	Sr	Y	Zr	Nb	Cs	Ba	Hf	Ta	Tl	Pb	Bi	Th	U
										Qinan Miocene Loess											
10.8	20GJ108	36.4	2.44	12.0	17.6	40.9	19.3	144	113	20.0	211	16.3	13.6	514	6.39	1.38	0.75	29.7	0.56	12.6	3.20
36.4	20GJ364	60.7	2.88	18.2	21.2	55.0	23.0	141	119	28.3	217	16.4	14.4	598	6.45	1.14	0.77	29.5	0.52	16.4	3.16
66.6	20ZW249	49.0	2.84	13.0	19.3	47.2	22.0	154	138	23.2	242	18.6	14.2	611	7.22	1.62	0.99	36.9	0.59	16.1	3.29
97.7	20ZW590	60.1	2.27	15.2	15.5	41.5	20.3	133	197	26.9	226	16.4	12.5	511	6.91	1.52	0.82	27.7	0.50	13.8	3.40
228.54	99QW2412	52.9	2.11	12.4	21.4	53.8	18.8	126	145	28.2	227	14.8	10.7	629	6.54	1.18	0.67	21.4	0.40	11.2	2.84
247.7	99QW3476	64.7	2.47	17.7	25.4	52.6	21.5	131	126	27.8	213	15.9	13.2	806	6.43	1.17	0.77	32.8	0.44	16.1	3.22
	average	54.0	2.50	14.7	20.1	48.5	20.8	138	140	25.8	223	16.4	13.1	612	6.66	1.33	0.79	29.7	0.50	14.4	3.18
										Qinan Miocene Soil											
0.8	20GJ8	54.6	2.57	14.4	20.7	46.6	23.0	161	126	23.2	234	18.5	15.4	580	7.00	1.52	0.88	31.4	0.63	15.5	3.48
17.6	20GJ176	59.1	2.71	18.0	20.1	57.8	23.0	137	113	25.5	214	17.0	15.1	587	6.51	1.27	0.78	29.1	0.53	15.8	3.23
55.2	20ZW135	62.7	2.58	16.9	18.2	47.8	21.5	133	112	26.3	232	17.0	14.4	585	6.95	1.23	0.77	28.1	0.52	15.6	3.32
83.5	20ZW448	66.2	2.63	17.2	19.9	50.3	22.6	117	125	24.9	231	16.4	13.7	561	6.84	1.21	0.76	30.8	0.55	16.7	3.32
159.12	99QW1690	78.2	2.79	17.6	26.9	48.4	24.0	153	146	28.6	227	18.3	13.8	807	6.58	1.43	0.86	41.6	0.55	14.9	3.24
166.3	99QW1763	55.6	2.18	14.0	14.9	41.3	19.4	118	117	28.6	219	14.4	11.6	404	6.46	1.04	0.67	20.1	0.39	12.7	3.16
	average	62.7	2.58	16.4	20.1	48.7	22.2	137	123	26.2	226	16.9	14.0	587	6.72	1.28	0.79	30.2	0.53	15.2	3.29
										Xifeng Pliocene Loess											
172.1	XFRC49	40.4	2.12	12.3	13.1	44.0	15.6	102	118	21.2	249	12.6	7.5	462	7.02	1.04	0.57	20.9	0.33	11.9	2.43
172.4	XFRC52	33.9	1.92	10.6	13.7	47.4	16.8	117	118	18.8	284	14.5	8.7	499	8.16	1.18	0.62	22.3	0.39	10.8	2.63
183.2	XFRC160	60.1	2.72	16.2	16.4	46.4	20.3	125	120	26.2	228	15.3	12.1	525	6.54	1.19	0.68	24.0	0.43	14.5	3.08
	average	44.8	2.25	13.0	14.4	45.9	17.6	115	119	22.1	254	14.1	9.4	495	7.24	1.13	0.63	22.4	0.38	12.4	2.71
										Xifeng Pliocene Soil											
174.9	XFRC77	56.8	2.64	15.0	15.5	38.7	18.7	119	120	26.7	267	15.4	10.0	470	7.76	1.22	0.64	22.4	0.41	13.9	3.16
176.3	XFRC91	48.4	2.23	14.6	17.3	42.2	20.1	130	113	26.1	257	17.2	11.3	539	7.63	1.76	0.73	25.6	0.46	13.2	2.99
197.3	XFRC301	56.7	2.39	15.6	19.3	46.2	22.1	146	115	24.4	243	17.6	12.6	548	7.40	1.47	0.83	29.0	0.52	14.0	3.12
	average	54.0	2.42	15.1	17.4	42.4	20.3	132	116	25.7	255	16.7	11.3	519	7.60	1.48	0.73	25.7	0.47	13.7	3.09
										Xifeng Pleistocene Loess											
8.5	XFC85	29.9	2.37	9.46	15.5	42.4	17.5	117	140	23.8	254	15.1	10.2	590	7.64	1.09	0.62	21.9	0.37	13.0	3.08
39.8	XF1213	29.1	2.16	9.58	15.6	36.5	17.7	127	151	19.7	255	23.7	9.8	546	7.37	1.84	0.73	24.1	0.41	11.4	3.04
45.3	XF1267	46.7	2.17	14.2	15.3	38.7	19.3	130	165	27.3	283	15.8	9.6	583	8.27	1.12	0.74	24.1	0.40	13.1	3.59
83.6	XF962	38.3	2.44	11.9	16.1	41.8	18.7	120	136	25.3	252	15.6	10.3	587	7.47	1.15	0.65	23.3	0.38	14.4	3.01
96.1	XF1113	41.5	2.67	11.0	15.6	39.4	18.1	115	134	23.2	281	15.5	9.3	505	7.90	1.23	0.67	23.8	0.39	13.9	2.87
98.3	XF1135	47.6	2.66	12.6	15.3	52.5	18.0	115	134	26.0	262	15.4	9.2	497	7.26	1.23	0.66	23.2	0.37	14.7	2.90
	average	38.8	2.41	11.5	15.5	41.9	18.2	121	143	24.2	265	16.9	9.7	552	7.65	1.28	0.68	23.4	0.39	13.4	3.08
										Xifeng Pleistocene Soil											
14.9	XFC149	36.9	2.42	9.77	15.7	41.0	18.8	132	168	22.4	276	16.7	11.7	557	8.51	1.34	0.61	25.9	0.44	12.6	2.82
41.1	XF1226	48.8	2.81	11.7	15.7	38.9	17.9	120	163	24.7	249	13.2	10.8	569	7.16	0.70	0.64	22.9	0.41	15.8	3.04
50.6	XF1313	38.7	2.18	10.9	17.4	45.2	19.5	144	147	25.0	242	16.9	12.0	591	7.25	1.37	0.72	26.2	0.44	14.4	3.29
85.9	XF1011	40.8	2.81	12.0	16.8	56.7	18.3	124	131	23.9	257	11.3	10.6	550	7.24	0.55	0.67	23.6	0.42	14.4	2.91
94.7	XF1099	29.7	2.58	10.7	16.3	44.9	19.7	138	128	23.6	270	16.6	11.5	558	8.24	1.31	0.62	27.1	0.45	11.7	2.64
100.7	XF12	44.7	2.43	12.9	16.2	44.2	20.2	138	137	24.6	246	16.7	11.4	572	7.55	1.33	0.64	26.1	0.44	12.3	2.42
	average	39.9	2.54	11.3	16.4	45.1	19.1	133	146	24.1	257	15.2	11.3	566	7.66	1.10	0.65	25.3	0.43	13.5	2.85
	UCC[b]	20.0	3.0	13.6	17.0	44.0	17.0	112	350	22.0	190	12.0	4.6	550	5.8	1.0	0.8	17.0	0.1	10.7	2.8

[a] In ppm, recalculated on a volatile-free basis.
[b] *Taylor and McLennan* [1985] and *McLennan* [2001].

with UCC with a stronger depletion for the Miocene samples (Figure 4b).

[12] Weathering processes are sequentially characterized by the early Na and Ca removal stage, the intermediate K removal stage and the more advanced Si removal stage [*Nesbitt et al.*, 1980]. These trends can be determined using the Al_2O_3-$CaO+Na_2O$-K_2O triangular diagram [*Nesbitt et al.*, 1980]. The plot for the loess and paleosol samples of different ages (Figure 4c) shows that all of them are in the early Na and Ca removal stage. However, the strongest Na and Ca depletion is observed for the Miocene paleosol samples.

Table 3. Rare Earth Element Concentrations of Eolian Sediments From Different Ages[a]

Depth (m)	Sample	La	Ce	Pr	Nd	Sm	Eu	Gd	Tb	Dy	Ho	Er	Tm	Yb	Lu	∑REE	La_N	Yb_N	La_N/Yb_N	Eu/Eu*
										Qinan Miocene Loess										
10.80	20GJ108	28.17	63.42	6.26	23.25	4.26	0.83	3.72	0.62	3.61	0.79	2.24	0.36	2.32	0.37	140.22	90.29	11.05	8.17	0.63
36.40	20GJ364	39.53	81.51	9.17	32.84	5.95	1.31	5.42	0.88	4.87	1.03	2.88	0.44	2.89	0.44	189.14	126.71	13.77	9.20	0.70
66.60	20ZW249	34.60	81.30	7.44	27.99	4.80	0.95	4.24	0.66	3.82	0.85	2.40	0.37	2.54	0.40	172.36	110.91	12.09	9.18	0.63
97.70	20ZW590	35.15	68.70	8.31	31.50	6.06	1.18	5.54	0.86	5.02	1.05	2.95	0.44	2.92	0.44	170.13	112.67	13.89	8.11	0.61
228.54	99QW2412	33.79	65.18	7.92	29.83	5.62	1.20	5.47	0.83	4.75	1.02	2.76	0.41	2.69	0.40	161.87	108.30	12.79	8.46	0.65
247.70	99QW3476	38.39	83.61	9.74	33.91	5.93	1.39	5.46	0.95	5.10	1.04	2.90	0.44	2.89	0.44	192.19	123.06	13.78	8.93	0.74
	average	34.94	73.95	8.14	29.89	5.44	1.14	4.98	0.80	4.53	0.96	2.69	0.41	2.71	0.41	170.98	111.99	12.90	8.67	0.66
										Qinan Miocene Soil										
0.80	20GJ8	36.11	73.35	8.28	30.74	5.35	1.08	4.85	0.78	4.40	0.92	2.62	0.40	2.66	0.40	171.95	115.75	12.67	9.13	0.64
17.60	20GJ176	35.37	76.32	8.03	27.63	4.94	1.09	4.56	0.78	4.52	0.97	2.69	0.42	2.82	0.42	170.56	113.37	13.45	8.43	0.69
55.20	20ZW135	35.94	76.65	8.60	29.60	5.31	1.11	4.80	0.85	4.77	0.99	2.81	0.44	2.93	0.44	175.23	115.20	13.97	8.25	0.66
83.50	20ZW448	38.03	86.54	9.54	32.92	5.91	1.27	5.12	0.87	4.71	0.99	2.79	0.44	2.90	0.44	192.49	121.89	13.83	8.82	0.69
159.12	99QW1690	39.50	91.07	9.34	35.52	6.53	1.36	5.91	0.90	5.21	1.05	2.91	0.45	2.91	0.43	203.09	126.61	13.87	9.13	0.66
166.30	99QW1763	31.81	61.48	7.26	25.88	4.80	1.09	4.62	0.80	4.47	0.96	2.68	0.42	2.74	0.40	149.41	101.95	13.04	7.82	0.70
	average	36.13	77.57	8.51	30.38	5.47	1.17	4.98	0.83	4.68	0.98	2.75	0.43	2.83	0.42	177.12	115.79	13.47	8.59	0.67
										Xifeng Pliocene Loess										
172.10	XFRC49	29.06	60.82	6.86	23.75	4.29	0.90	3.85	0.64	3.68	0.78	2.24	0.35	2.32	0.36	139.90	93.13	11.04	8.44	0.67
172.40	XFRC52	27.43	59.80	6.25	23.24	4.02	0.84	3.46	0.57	3.46	0.73	2.15	0.35	2.23	0.34	134.87	87.91	10.64	8.26	0.67
183.20	XFRC160	35.87	73.54	8.25	30.83	5.56	1.11	4.93	0.81	4.37	0.97	2.70	0.42	2.75	0.42	172.51	114.96	13.08	8.79	0.64
	average	30.78	64.72	7.12	25.94	4.62	0.95	4.08	0.67	3.84	0.83	2.37	0.37	2.43	0.37	149.09	98.67	11.59	8.50	0.66
										Xifeng Pliocene Soil										
174.90	XFRC77	35.74	73.66	8.64	30.62	5.63	1.12	4.94	0.81	4.61	1.00	2.76	0.43	2.84	0.44	173.24	114.55	13.54	8.46	0.64
176.30	XFRC91	32.95	70.06	7.71	28.50	5.30	1.05	4.97	0.81	4.81	1.03	2.84	0.44	2.83	0.44	163.74	105.62	13.47	7.84	0.62
197.30	XFRC301	34.41	73.29	8.02	30.14	5.22	1.06	4.87	0.75	4.56	0.97	2.76	0.42	2.79	0.43	169.69	110.30	13.31	8.29	0.64
	average	34.37	72.33	8.12	29.76	5.38	1.08	4.92	0.79	4.66	1.00	2.79	0.43	2.82	0.43	168.89	110.15	13.44	8.20	0.63
										Xifeng Pleistocene Loess										
8.50	XFC85	30.69	71.36	7.26	25.17	4.46	0.96	4.24	0.72	3.97	0.83	2.35	0.38	2.49	0.36	155.23	98.37	11.83	8.31	0.66
39.80	XF1213	28.77	58.28	6.46	21.31	4.01	0.79	3.78	0.57	3.39	0.73	2.11	0.34	2.28	0.36	133.19	92.21	10.88	8.48	0.61
45.30	XF1267	37.35	77.85	8.76	33.18	6.15	1.16	5.15	0.85	5.06	1.08	2.95	0.46	3.10	0.48	183.58	119.70	14.74	8.12	0.61
83.60	XF962	34.88	74.63	8.36	29.37	5.21	1.14	4.74	0.80	4.49	0.96	2.70	0.42	2.74	0.41	170.83	111.78	13.03	8.58	0.69
96.10	XF1113	33.57	72.30	7.97	28.23	5.24	1.03	4.79	0.74	4.23	0.88	2.46	0.39	2.50	0.38	164.71	107.59	11.91	9.03	0.62
98.30	XF1135	35.93	76.66	9.07	31.10	6.06	1.10	5.22	0.82	4.78	1.01	2.78	0.43	2.82	0.43	178.22	115.18	13.45	8.56	0.58
	average	33.53	71.85	7.98	28.06	5.19	1.03	4.65	0.75	4.32	0.91	2.56	0.40	2.65	0.40	164.29	107.47	12.64	8.52	0.63
										Xifeng Pleistocene Soil										
14.90	XFC149	34.11	85.06	7.86	29.47	5.18	1.04	5.02	0.76	4.36	0.90	2.42	0.38	2.31	0.37	179.24	109.31	10.98	9.96	0.62
41.10	XF1226	38.36	83.85	8.74	31.09	5.50	1.06	4.81	0.78	4.45	0.95	2.65	0.42	2.76	0.42	185.84	122.94	13.15	9.35	0.61
50.60	XF1313	38.44	86.82	8.66	33.11	5.96	1.17	5.67	0.87	4.77	0.97	2.73	0.39	2.68	0.40	192.65	123.21	12.77	9.65	0.61
85.90	XF1011	33.35	73.02	8.07	27.54	4.95	0.97	4.53	0.72	4.23	0.90	2.52	0.40	2.58	0.39	164.15	106.88	12.28	8.70	0.61
94.70	XF1099	30.83	75.25	6.90	25.78	4.53	0.92	4.42	0.73	4.44	0.93	2.67	0.41	2.55	0.41	160.78	98.83	12.13	8.15	0.62
100.70	XF12	36.42	77.26	8.25	30.67	5.40	1.09	4.86	0.76	4.53	0.97	2.66	0.41	2.57	0.40	176.25	116.73	12.22	9.55	0.64
	average	35.25	80.21	8.08	29.61	5.25	1.04	4.88	0.77	4.46	0.94	2.61	0.40	2.57	0.40	176.49	112.98	12.26	9.23	0.62
	UCC[b]	39	64	7.1	26	4.5	0.88	3.8	0.64	3.5	0.8	2.3	0.33	2.2	0.32	146	96.8	10.5	9.22	0.65

[a] In ppm, recalculated on a volatile-free basis.
[b] *Taylor and McLennan* [1985].

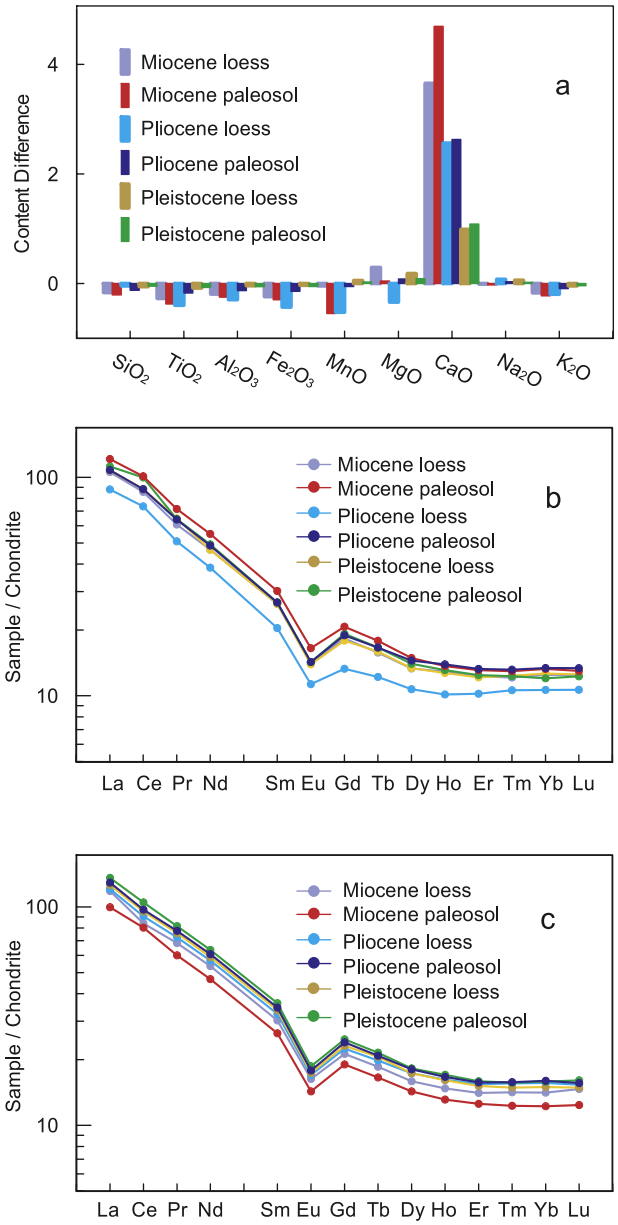

Figure 2. Results of test experiments on the effect of carbonate leaching using 1mol/l HAc. (a) Differences of major elemental content normalized by UCC [*Taylor and McLennan*, 1985; *McLennan*, 2001] for pretreated and posttreated samples. (b) Chondrite-normalized REE distribution patterns for pretreated samples. (c) Chondrite-normalized REE distribution patterns for posttreated samples. The experiments used six Pleistocene samples, four Pliocene samples from Xifeng, and twenty Miocene samples from QA-I. All of the results are recalculated on a volatile-free basis.

[13] Chemical index of alteration (CIA) [*Nesbitt and Young*, 1982] is widely used to evaluate the chemical weathering of terrestrial sediments. It is defined as CIA = $Al_2O_3/(Al_2O_3 + CaO^* + Na_2O + K_2O) \times 100$ (in molar proportions, CaO* is the amount of CaO in silicates). Using the CaO content after removing carbonate, CIA ranges from 63.60 to 70.51 (average 67.89) for the Miocene loess samples, from 66.73 to 72.14 (average 69.56) for the Miocene paleosol samples, from 63.33 to 70.70 (average 67.19) for the Pliocene loess samples, from 66.20 to 70.33 (average 68.30) for the Pliocene paleosol samples, from 61.31 to 68.36 (average 64.26) for the Pleistocene loess samples and from 63.23 to 69.22 (average 66.34) for the Pleistocene paleosol samples (Table 1). The CIA values in the Miocene loess samples are significantly

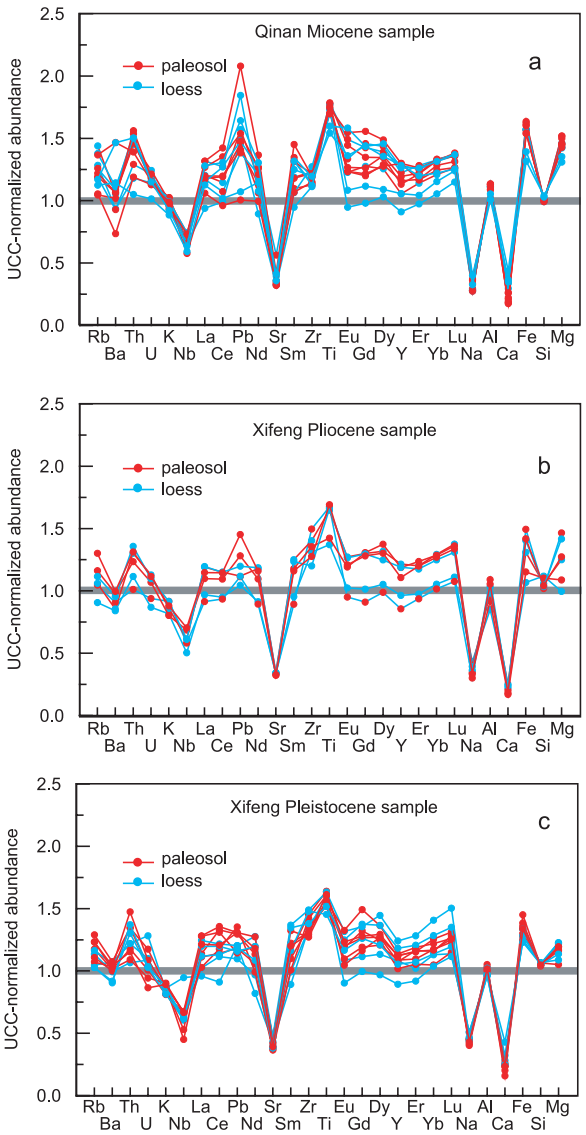

Figure 3. UCC-normalized abundances for the loess and paleosol samples of different ages. (a) Qinan Miocene sample, (b) Xifeng Pliocene sample, and (c) Xifeng Quaternary sample. The UCC values are from *Taylor and McLennan* [1985] and *McLennan* [2001].

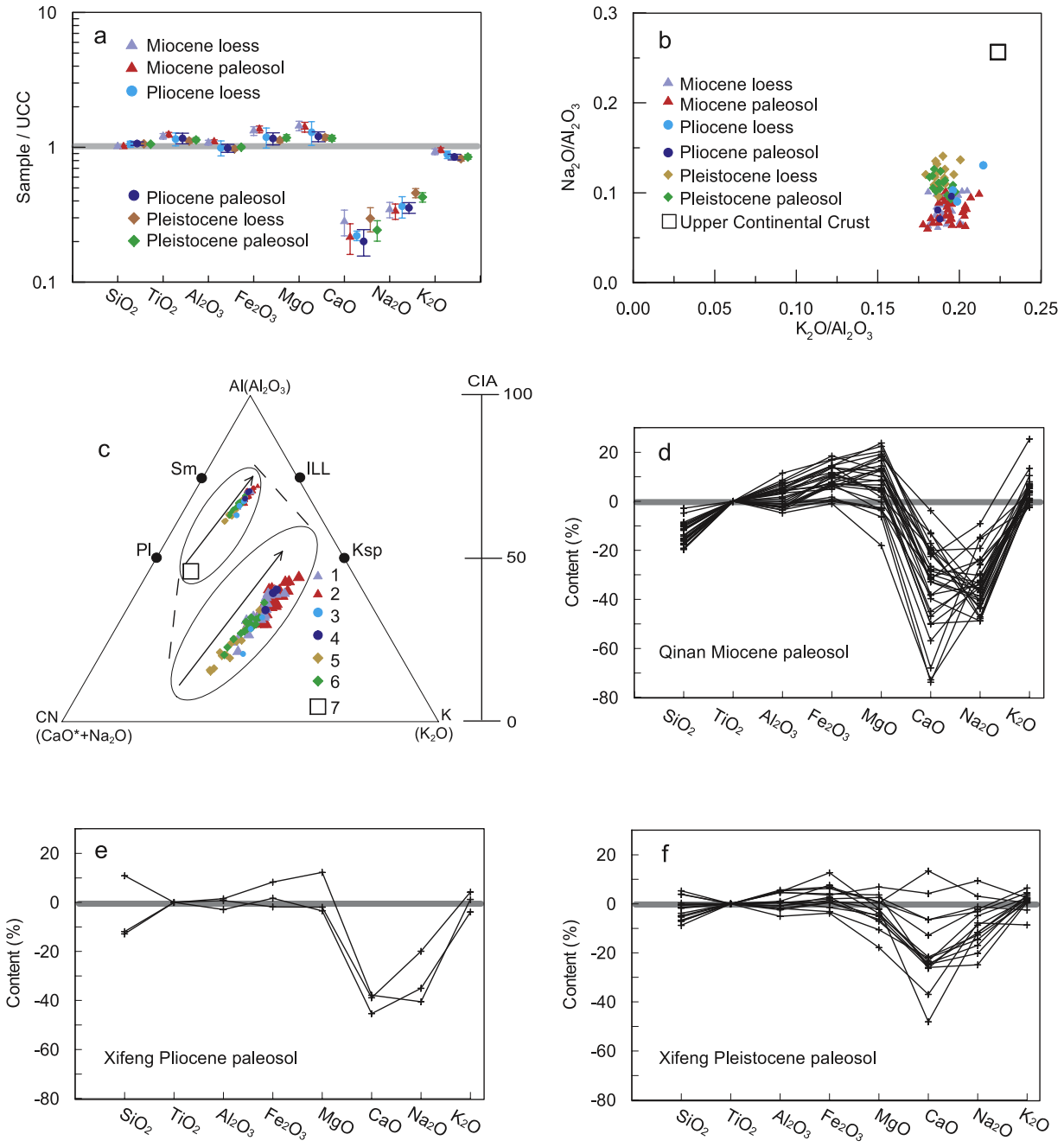

Figure 4. (a) UCC-normalized major element comparison diagram of the studied samples. (b) Na_2O/Al_2O_3 versus K_2O/Al_2O_3 diagrams for samples of different ages. (c) A-CN-K (Al_2O_3-(CaO*+Na_2O)-K_2O) diagrams of the Miocene and Plio-Pleistocene samples and their chemical index of alteration (CIA). (Sample 1, Miocene loess sample; sample 2, Miocene paleosol sample; sample 3, Pliocene loess sample; sample 4, Pliocene paleosol sample; sample 5, Pleistocene loess sample; sample 6, Pleistocene paleosol sample; and sample 7, upper continental crust [*Taylor and McLennan*, 1985; *McLennan*, 2001]. Sm, smectite; ILL, illite; Ksp, potassium feldspar; Pl, plagioclase. CaO* is the amount of CaO incorporated in the silicate fraction of the samples.) (d) Results of elemental mass balance calculations for thirty Miocene paleosol samples. (e) Results of elemental mass balance calculations for three Pliocene paleosol samples. (f) Results of elemental mass balance calculation for fifteen Quaternary paleosol samples.

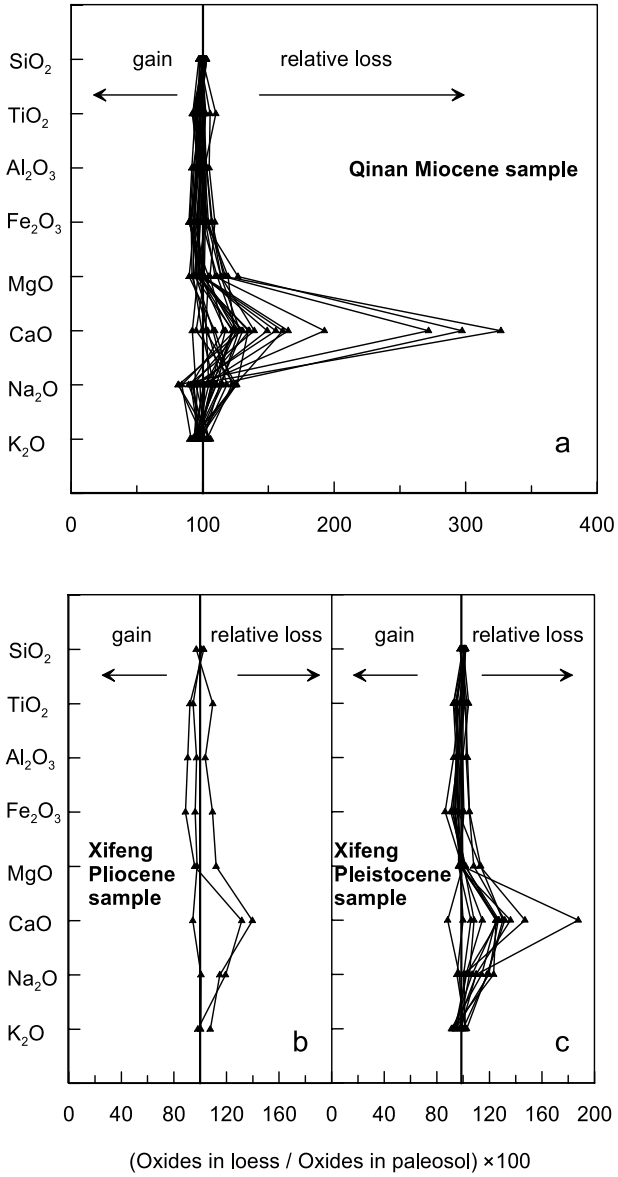

Figure 5. Mean elemental gain-loss calculations between loess and paleosol for (a) Miocene, (b) Pliocene, and (c) Pleistocene sequences. The Plio-Pleistocene calculations show little change, whereas a more pronounced gain-loss is observed in the Miocene sequence.

higher than the UCC value of 50 [*Taylor and McLennan*, 1985; *McLennan*, 2001]. For comparison, modern soils and major river particulates show a wide range of CIA values [*McLennan*, 1993]. Earlier studies show that systematic progression in alteration minerals tracks incipient (CIA = 50–60), to intermediate(CIA = 60–80), to extreme (CIA > 80) chemical weathering [*Fedo et al.*, 1995].

[14] To further evaluate the differences in element abundance between the Miocene paleosol and loess samples, and between the Miocene paleosols and the Pliocene- Pleistocene paleosols, a mass balance method [*Nesbitt*, 1979] is applied to the studied samples. We assume a similar initial composition for the paleosol and loess layers, and then use the average content of major elements of the thirty Miocene loess samples as the initial composition of paleosol layers (p). We select TiO_2 as an invariant oxide (I) because of its immobile behavior during weathering and pedogenesis [*Nesbitt*, 1979; *Nesbitt and Markovics*, 1997]. The changes in the content of any element X in a paleosol sample (s) is given by the equation % change = $((X^s/I^s)/(X^p/I^p) - 1) \times 100$. The results of gain-loss calculations for the thirty Miocene paleosol samples (Figure 4d) show small changes of SiO_2 and K_2O (<20%), slight gains for Al_2O_3, Fe_2O_3 and MgO (<24%), and significant losses for Na_2O (~48%) and CaO (~74%). There are smaller gain-loss percentages in Plio-Pleistocene paleosols compared with the Miocene paleosols. The highest loss for CaO in Pliocene and Pleistocene paleosol samples is

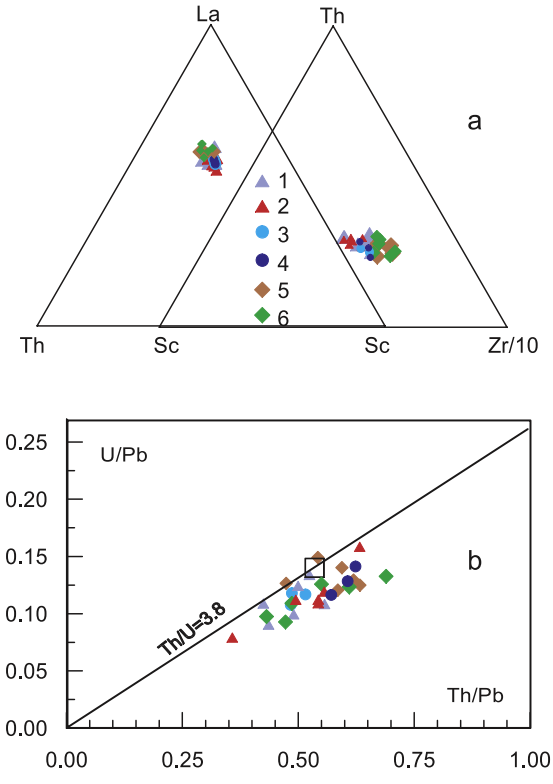

Figure 6. (a) La-Th-Sc and Th-Sc-Zr/10 discrimination diagrams for the samples of different ages. Symbols are the same as Figure 4c. (b) U/Pb versus Th/Pb ratios for samples of different ages.

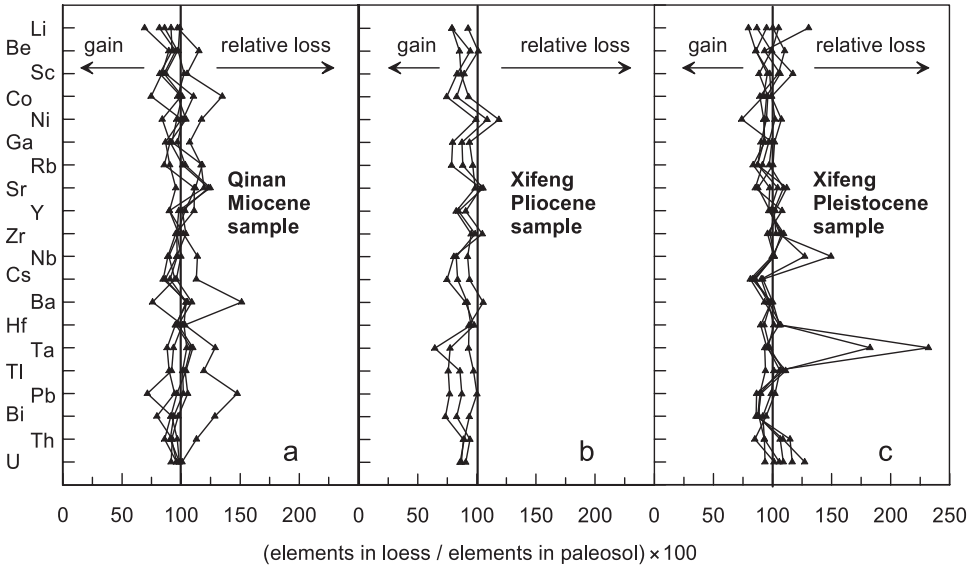

Figure 7. Mean trace element gain-loss calculations between loess and paleosol for the (a) Miocene, (b) Pliocene, and (c) Pleistocene sequences.

~45% and ~48%, respectively, less than that for the Miocene samples (~74%) (Figures 4d–4f).

[15] The stronger quantitative change in major element abundances in the Miocene paleosol samples also can be confirmed by gain-loss calculations [*Garrels and Mackenzie*, 1971]. We assumed the initial major element composition of a given Miocene (Pliocene and Pleistocene) paleosol layer is identical to the average composition of the Miocene (Pliocene and Pleistocene, respectively) loess samples. We then performed gain-loss calculations for the three epochs (Figure 5). The Plio-Pleistocene paleosols show little gain or loss, with the most significant change being the CaO loss in the Miocene paleosols. Highest loss is observed for three samples from the bottom section of the early Miocene (Figure 5a). These reinforce the above results deduced using the mass balance method.

3.2. Trace Element Characteristics

[16] Trace element (elements with a content <0.1%) data and their average content for the samples studied are given in Table 2. Comparisons for the samples of different ages (Figures 3a–3c) show a strong similarity irrespective of age, with only slight differences for Ce, Pb and Zr. The values also resemble the average of UCC [*Taylor and McLennan*, 1985; *McLennan*, 2001]. The La-Th-Sc and Th-Sc-Zr/10 discrimination diagram (Figure 6a) of these deposits also exhibit no significant changes related to age. These elements are usually believed to be conservative and reliable indices of sediment provenance [*Bhatia and Crook*, 1986]. Therefore, no significant change in source area during Miocene and Plio-Pleistocene can be inferred from these results.

[17] The UCC-normalized patterns (Figure 3) of all the samples exhibit consistent trace element trends. Compared with the composition of the average UCC, all of the eolian samples in China show slightly lower Sr. The plot of U/Pb versus Th/Pb (Figure 6b) indicates a substantial removal of U compared with UCC. Among the three sets of samples (Miocene, Pliocene and Pleistocene), the Miocene samples are slightly lower in Zr and Hf content and higher in Cs content (Table 2).

[18] In order to examine the quantitative change in trace element abundances between loess and paleosols, a gain-loss calculation [*Garrels and Mackenzie*, 1971] was also applied (Figure 7). Despite the different ages, there was little change in trace element abundance between loess and paleosol in any of the sample sets.

3.3. Rare Earth Elemental Characteristics

[19] The REE content of clastic rocks is mainly controlled by the lithologic composition in the source area [*Fleet*, 1984; *McLennan*, 1989]. It is therefore a better indicator of the sources and depositional processes of eolian sediments [*Gallet et al.*, 1998; *Ding et al.*, 2001].

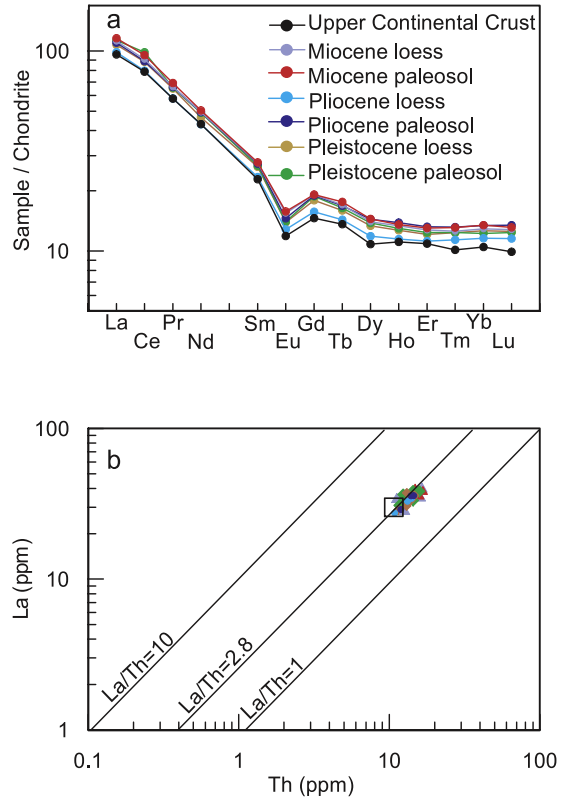

Figure 8. (a) Chondrite-normalized REE distribution patterns for the studied samples and comparisons with UCC [*Taylor and McLennan*, 1985]. (b) La versus Th diagram showing uniform values for samples of different ages and the similarity to the "continental" La/Th ratios. Symbols are the same as Figure 4c.

[20] The data for REEs are given in Table 3. The REE distribution patterns of the Miocene loess samples (Figure 8a) are remarkably similar to those of the Pliocene and Pleistocene samples, with enriched LREE (light REEs) and relatively flat HREE (heavy REEs) profiles, a restricted range of La_N/Yb_N ratios (7–10) and a constant negative Eu anomaly. All of the values (Table 3) are also close to the average compositions of UCC [*Taylor and McLennan*, 1985].

[21] Eu fractionation relative to other REEs is unlikely to occur during weathering and sedimentation processes [*McLennan*, 1989]. Only strong enrichment of plagioclase could lead to large changes of Eu/Eu* ratios [*Condie et al.*, 1995] (Eu* is the theoretical value of Eu, $Eu^* = (Sm_N + Gd_N)/2$). This ratio for all the loess samples in China varies between 0.6 and 0.7 despite the age differences.

[22] *Taylor and McLennan* [1985] used La/Th value (2.8 ± 0.2 for fine-grained sediments in average) to estimate the deviations of sediments from UCC composition. This ratio shows no clear distinction between the whole-rock and size fractions derived from it, and so would be little affected by sedimentary sorting [*Gallet et al.*, 1998]. The La/Th ratios (Figure 8b) of the Miocene loess samples are almost consistent with those of the Plio-Pleistocene loess samples, and are all close to the ratio of UCC.

3.4. Provenance and Paleoclimate Implications

[23] Our results reveal an overall similarity of geochemical characteristics between the Miocene continental loess in northern China and the UCC [*Taylor and McLennan*, 1985; *McLennan*, 2001] (Figures 3 and 8). This same feature has been noted in previous studies of Plio-Pleistocene eolian deposits in northern China [*Liu*, 1985; *Wen*, 1989; *Gallet et al.*, 1996, 1998; *Ding et al.*, 1998b, 2001; *Chen et al.*, 2001]. It indicates that the loess materials of the past 22 Ma were derived from extensive areas and had experienced numerous upper crustal recycling processes. Our results reinforce the earlier conclusion that the average chemical crustal composition of UCC can be obtained from eolian deposits [*Taylor and McLennan*, 1985; *Gallet et al.*, 1998]. They also suggest that the Miocene loess in northern China, like the younger eolian deposits from the region [*Gallet et al.*, 1998], can provide an equally good proxy for UCC. This constitutes yet more evidence for the eolian origin of the Miocene deposits considered here.

[24] However, our results do reveal several differences between the composition of the Miocene loess samples and that of UCC. These include the slight TiO_2 positive and Na_2O, CaO negative anomalies (Figure 4a), the slightly lower Sr content (Figure 3), the depletions of Na and U shown by the plots of Na_2O/Al_2O_3 versus K_2O/Al_2O_3 (Figure 4b) and U/Pb versus Th/Pb (Figure 6b). These differences, already noted in respect of the younger eolian deposits in northern China [*Gallet et al.*, 1998], suggest that the loess materials in northern China must have experienced many cycles involving processes of sedimentary differentiation with moderate chemical weathering in the source areas prior to their transportation to the Loess Plateau region. Earlier studies suggest that Ti is least affected by weathering solutions and usually resides in stable heavy minerals such as anatase, pyromelane and rutile, leading to higher

TiO_2 content in eolian deposits [*Wen*, 1989; *Gallet et al.*, 1998]. During the alteration of igneous to sedimentary rocks, clays and carbonate minerals form, Na is removed and transported into the oceans, and K is retained in shales [*Garrels and Mackenzie*, 1971]. Sr behaves like Ca, which is lost significantly in initially weathered rocks and continues to be lost during later stages of weathering [*Dasch*, 1969].

[25] In comparison with the other less extensive loess formations of the world [*Taylor et al.*, 1983], one of the distinct features of the eolian deposits in northern China is the higher Cs, lower Zr and Hf concentrations. This may be linked to the desert origin of the eolian dust in northern China, compared with the closer river valley or glacial origin of the other loesses. Zr and Hf are mainly contained in a heavy mineral zircon which is normally enriched relative to upper crustal abundances during the loess-forming process [*Taylor et al.*, 1983]. Earlier examination indicated that zircon is more abundant in the coarse fraction of loess [*Liu*, 1985]. In contrast Cs is apt to concentrate in fine particles, since during continental weathering, Cs is easily fixed in continental profiles by exchange and absorption onto secondary clays, hence its affinity with fine particles [*Nesbitt et al.*, 1980]. The higher Cs, lower Zr and Hf concentrations in the eolian deposits in China may be attributable to the long transportation trajectory of eolian dust from the remote deserts which may lead to grain size and mineral sorting [*Ding et al.*, 1999], and consequently to higher Cs, and lower Zr and Hf concentrations in finer and remotely deposited dust. In contrast, these sorting processes are minimized for loess closer to the source of origin. The higher Cs and lower Zr and Hf content could thus be regarded as an indication of a desert origin for loess.

[26] Another prominent geochemical feature revealed in our study is the overall similarity between the Miocene, Pliocene and Pleistocene loess samples. This would also suggest broadly similar source areas and dust-transporting trajectories throughout the past 22 Ma in terms of geographical patterns. The interpretation is particularly supported by the relatively narrow range of values for the Eu/Eu* ratio between 0.6 and 0.7 (Table 3) for all the analyzed samples as this ratio appears to be sensitive to provenance differences: ~0.7 for Spitsbergen loess, 0.53–0.67 for European loess and 0.74–0.83 for loess in Argentina [*Gallet et al.*, 1998]. Further information comes from the La-Th-Sc and Th-Sc-Zr/10 discrimination diagram (Figure 6a). La, Th, Sc and Zr are relatively insoluble and are not significantly fractionated during weathering, erosion, transportation and deposition [*Taylor and McLennan*, 1985]. All the samples of different ages have closely comparable values, indicating that the Miocene and Plio-Pleistocene eolian deposits were derived from broadly similar source areas through comparable dust transporting processes. This is consistent with the spatial reconstructions of Cenozoic climates [*Liu and Guo*, 1997; *Sun and Wang*, 2005; *Zhang and Guo*, 2005; *Guo et al.*, 2008] showing that a pattern similar to the present-day monsoon-dominated climate was already formed by the early Miocene. It also supports the view that the Asian winter monsoon was the main dust carrier since the early Miocene [*Guo et al.*, 2002].

[27] The observed differences in geochemical characteristics between the Miocene loess and younger eolian deposits include the slightly lower SiO_2 and Na_2O content, higher Al_2O_3, Fe_2O_3, K_2O and LOI content (Table 1), the slightly lower Zr and Hf and higher Cs content (Table 2). These are attributable to two factors. Earlier studies showed that the SiO_2 content in Chinese loess is negatively correlated with grain size [*Liu et al.*, 1995; *Peng and Guo*, 2001; *Guo et al.*, 2004] and that magnesium and iron minerals are apt to congregate in the fine fraction because of a sorting effect [*Nesbitt et al.*, 1996]. The above features of the Miocene loess are partly attributable to their finer median grain size, 7~12 μm versus 15~22 μm for the Pleistocene loess [*Qiao et al.*, 2006] due to weaker transporting winds in the Miocene [*Guo et al.*, 2002; *Qiao et al.*, 2006] and remoter sources compared with the Plio-Pleistocene loess, as suggested by the lower Zr, Hf and higher Cs content of the Miocene samples. This is consistent with the lower loess accumulation rates during the Miocene [*Guo et al.*, 2002], an indication of less arid conditions in the source region. Another factor would be the generally warmer climates at global scale in the Miocene as documented by the marine $\delta^{18}O$ records [*Zachos et al.*, 2001] because warmer climates would lead to stronger weathering in both source and depositional regions. The higher CIA values (68.72) in the Miocene samples are consistent with the likely implications of the global climate during that period.

[28] Comparison between samples from the Miocene loess and intervening paleosol layers (Figures 4d and 5a) reveals significantly stronger losses of

CaO in the paleosol layers, with smaller changes in SiO_2 and K_2O (<20%). Ca is mainly concentrated in carbonate and plagioclase. As carbonate was leached before chemical analysis, the stronger loss of CaO in the paleosol layers, particularly for the early Miocene samples, indicates that more plagioclase decomposed in the paleosol than in the loess layers, which implies stronger chemical weathering during the formation of the paleosol layers than during the deposition of the intervening loess. These results confirm the relatively warmer/more humid conditions during the soil-forming intervals and the relatively drier/cooler conditions during the intervals of loess deposition. The alternations of more than 230 soil-loess pairs in the QA-I Miocene sequence are reflective of the summer and winter monsoon changes within the orbital band [*Guo et al.*, 2002]. Besides, comparison between Figure 4d and Figures 4e and 4f, also between Figure 5a and Figures 5b and 5c, shows that there was much greater loss of CaO from the Miocene paleosol samples (with a maximum of 74%) than is recorded in the Plio-Pleistocene sequences (with the maxima of 45%, 48%, respectively). It can be concluded that chemical weathering was stronger during the Miocene, especially the early Miocene, than during the Plio-Pleistocene. However, the Na-Ca removal stage of the Miocene paleosols, as characterized by the plot of Na_2O/Al_2O_3 versus K_2O/Al_2O_3 (Figure 4b), the Al_2O_3-CaO+Na_2O-K_2O triangular diagram (Figure 4c) and the CIA values, clearly indicates moderate chemical weathering typical of semiarid and subhumid regions. Despite the drastic global climate changes from the early Miocene to the Pleistocene [*Zachos et al.*, 2001], the degree of chemical weathering indicated by the stage of Ca-Na removal for all the studied samples definitively indicates a semiarid and subhumid climate regime in the Loess Plateau in northern China since the early Miocene.

4. Conclusions

[29] Our geochemical analyses on the Miocene loess and paleosol samples and the comparison with the younger eolian deposits in northern China significantly enhance the range of geochemical data available for the key QA-I section and for evaluating the extent to which and the way in which they correspond to or differ from those from the more extensively studied Pliocene and Pleistocene sequences. They lead to the following conclusions.

[30] The results show a strong similarity in geochemical characteristics between the Miocene loess and the average UCC, indicating that the dust materials were all derived from well-mixed sedimentary protoliths which underwent numerous upper crustal recycling processes. Their minor differences are attributable to the sedimentary differentiation processes and to moderate chemical weathering of the dust materials mostly occurring prior to their deposition.

[31] The broadly uniform geochemical characteristic of the eolian deposits of different ages support the interpretation regarding similar dust source areas and transporting trajectories over the past 22 Ma. The slight differences between the Miocene and Plio-Pleistocene loess are essentially attributable to the finer grain size and stronger predepositional and postdepositional chemical weathering associated with the weaker winter monsoon, remoter sources and generally warmer climate conditions during the Miocene. The higher Cs, and lower Zr and Hf content in the eolian deposits in northern China compared with loess sequences elsewhere in the world may be regarded as a feature typical of loess with a desert origin.

[32] The stronger chemical weathering of the Miocene paleosol layers indicates relatively warmer/more humid climatic conditions during the soil-forming intervals with a stronger summer monsoon. The alternations of more than 230 soil-loess pairs in the QA-I Miocene sequence are reflective of the summer (warm/moist) and winter (dry/cold) monsoon changes within the orbital band [*Guo et al.*, 2002]. However, all the geochemical characteristics consistently define a degree of chemical weathering at the Na-Ca removal stage [*Nesbitt et al.*, 1980] typical of semiarid and subhumid regions. These indicate that a semiarid and subhumid climate regime was already established by the early Miocene and has been maintained over the past 22 Ma.

Acknowledgments

[33] This study was supported by the Chinese Academy of Sciences (KZCX2-YW-117), the National Natural Science Foundation of China (40730104), and the 973 Project (2004CB720203). Sincerest thanks are extended to Denis Rousseau and an anonymous reviewer for the constructive reviews of the manuscript.

References

An, Z., J. Kutzbach, W. Prell, and S. Porter (2001), Evolution of Asian monsoons and phased uplift of the Himalaya-Tibe-

tan Plateau since Late Miocene times, *Nature*, *411*, 62–66, doi:10.1038/35075035.

Bhatia, M. R., and K. A. W. Crook (1986), Trace element characteristics of graywackes and tectonic discrimination of sedimentary basins, *Contrib. Mineral. Petrol.*, *92*, 181–193, doi:10.1007/BF00375292.

Chen, J., H. Wang, and H. Lu (1996), Behaviors of REE and other trace elements during pedological weathering-evidence from chemical leaching of loess and paleosol from the Luochuan section in central China (in Chinese with English abstract), *Dizhi Xuebao*, *70*, 61–72.

Chen, J., J. Ji, G. Qiu, and H. Lu (1998), Geochemical studies on the intensity of chemical weathering in Luochuan loess-paleosol sequence, China, *Sci. China, Ser. D*, *41*, 235–241.

Chen, J., Z. An, L. Liu, J. Ji, J. Yang, and Y. Chen (2001), Variations in chemical compositions of the eolian dust in Chinese Loess Plateau over the past 2.5 Ma and chemical weathering in the Asian inland, *Sci. China, Ser. D*, *44*, 403–413.

Condie, K., J. Dengate, and R. Cullers (1995), Behavior of rare earth elements in a paleoweathering profile on granodiorite in the Front Range, Colorado, USA, *Geochim. Cosmochim. Acta*, *59*, 279–294, doi:10.1016/0016-7037(94)00280-Y.

Dasch, E. (1969), Strontium isotopes in weathering profiles, deep-sea sediments, and sedimentary rocks, *Geochim. Cosmochim. Acta*, *33*, 1521–1552, doi:10.1016/0016-7037(69)90153-7.

Ding, Z., J. Sun, R. Zhu, and B. Guo (1997), Eolian origin of the red clay deposits in the Loess Plateau and implication for Pliocene climatic change (in Chinese with English abstract), *Quat.*, *2*, 147–156.

Ding, Z., J. Sun, S. Yang, and T. Liu (1998a), Preliminary magnetostratigraphy of a thick eolian red clay-loess sequence at Lingtai, the Chinese Loess Plateau, *Geophys. Res. Lett.*, *25*, 1225–1228, doi:10.1029/98GL00836.

Ding, Z., J. Sun, T. Liu, R. Zhu, S. Yang, and B. Guo (1998b), Wind-blown origin of the Pliocene red clay formation in the central Loess Plateau, *Earth Planet. Sci. Lett.*, *161*, 135–143, doi:10.1016/S0012-821X(98)00145-9.

Ding, Z., J. Sun, N. W. Rutter, D. Rokosh, and T. Liu (1999), Changes in sand content of loess deposits along a north-south transect of the Chinese loess plateau and the implication for desert variation, *Quat. Res.*, *52*, 56–62, doi:10.1006/qres.1999.2045.

Ding, Z., J. Sun, S. Yang, and T. Liu (2001), Geochemistry of the Pliocene red clay formation in the Chinese Loess Plateau and implication for its origin, source provenance and paleoclimate change, *Geochim. Cosmochim. Acta*, *65*, 901–913, doi:10.1016/S0016-7037(00)00571-8.

Fedo, C., H. Nesbitt, and G. Young (1995), Unraveling the effects of potassium metasomatism in sedimentary rocks and paleosols, with implications for paleoweathering conditions and provenance, *Geology*, *23*, 921–924, doi:10.1130/0091-7613(1995)023<0921:UTEOPM>2.3.CO;2.

Fleet, A. (1984), Aqueous and sedimentary geochemistry of the rare earth elements, in *Rare Earth Element Geochemistry*, edited by P. Henderson, pp. 331–373, Elsevier, Amsterdam.

Gallet, S., B. Jahn, and M. Torii (1996), Geochemical characterization of loess-paleosol sequence from the Luochuan section, China and its paleoclimatic implications, *Chem. Geol.*, *133*, 67–88, doi:10.1016/S0009-2541(96)00070-8.

Gallet, S., B. Jahn, B. Lanoe, A. Dia, and E. Rossello (1998), Loess geochemistry and its implications for particle origin and composition of the upper continental crust, *Earth Planet. Sci. Lett.*, *156*, 157–172, doi:10.1016/S0012-821X(97)00218-5.

Garrels, R., and E. T. Mackenzie (1971), *Evolution of Sedimentary Rocks*, Norton, New York.

Gu, Z., Z. Ding, S. Xiong, and T. Liu (1999), A seven million geochemical record from Chinese red-clay and loess-paleosol sequence: Weathering and erosion in northwestern China (in Chinese with English abstract), *Quat. Sci.*, *4*, 357–365.

Gu, Z., J. Hao, and T. Liu (2000), Progress in geochemical research on the loess and other Quaternary deposits in China (in Chinese with English abstract), *Quat. Sci.*, *20*, 41–55.

Guo, Z., S. Peng, Q. Hao, P. Biscaye, and T. Liu (2001), Origin of the Miocene-Pliocene Red-Earth Formation at Xifeng in northern China and implications for paleoenvironment, *Palaeogeogr. Palaeoclimatol. Palaeoecol.*, *170*, 11–26, doi:10.1016/S0031-0182(01)00235-8.

Guo, Z., W. Ruddiman, Q. Hao, H. Wu, Y. Qiao, R. Zhu, S. Peng, J. Wei, B. Yuan, and T. Liu (2002), Onset of Asian desertification by 22 Myr ago inferred from loess deposits in China, *Nature*, *416*, 159–163, doi:10.1038/416159a.

Guo, Z., S. Peng, Q. Hao, P. Biscaye, Z. An, and T. Liu (2004), Late Miocene-Pliocene development of Asian aridification as recorded in the Red-Earth Formation in northern China, *Global Planet. Change*, *41*, 135–145, doi:10.1016/j.gloplacha.2004.01.002.

Guo, Z., et al. (2008), A major reorganization of Asian climate by the early Miocene, *Clim. Past.*, *4*, 153–174.

Hao, Q., and Z. Guo (2007), Magnetostratigraphy of an early-middle Miocene loess-soil sequence in the western Loess Plateau of China, *Geophys. Res. Lett.*, *34*, L18305, doi:10.1029/2007GL031162.

Ji, J., and J. Chen (2000), An EPR study on the chemical form of Mn^{2+} in the Chinese loess samples, *Spectrosc. Lett.*, *32*, 202–209.

Kukla, G., Z. An, J. Melice, J. Gavin, and J. Xiao (1990), Magnetic susceptibility record of Chinese Loess, *Trans. R. Soc. Edinburgh Earth Sci.*, *81*, 263–288.

Li, F., N. Wu, Y. Pei, Q. Hao, and D. Rousseau (2006), Wind-blown origin of Dongwan late Miocene–Pliocene dust sequence documented by land snail record in western Chinese Loess Plateau, *Geology*, *34*, 405–408, doi:10.1130/G22232.1.

Li, F., D. Rousseau, N. Wu, Q. Hao, and Y. Pei (2008), Late Neogene evolution of the east Asian monsoon revealed by terrestrial mollusk record in Western Chinese Loess Plateau: From winter to summer dominated sub-regime, *Earth Planet. Sci. Lett.*, *274*, 439–447, doi:10.1016/j.epsl.2008.07.038.

Liu, J., Z. Guo, Q. Hao, S. Peng, Y. Qiao, B. Sun, and J. Ge (2005), Magnetostratigraphy of the Miziwan Miocene eolian deposits in Qin'an country (Gansu Province) (in Chinese with English abstract), *Quat. Sci.*, *25*, 503–509.

Liu, J., Z. Guo, Y. Qiao, Q. Hao, and B. Yuan (2006), Eolian origin of the Miocene loess-soil sequence at Qin'an, China: Evidence of quartz morphology and quartz grain-size, *Chin. Sci. Bull.*, *51*, 117–120, doi:10.1007/s11434-005-0811-8.

Liu, L., H. Wang, Y. Chen, and J. Chen (2002), Chemical leaching of loess deposits in China and its implications for carbonate composition (in Chinese with English abstract), *Acta Petrol. Mineral.*, *21*, 69–75.

Liu, T. (1985), *Loess and the Environment*, China Ocean Press, Beijing.

Liu, T., and Z. Guo (1997), Geological environment in China and global change, in *Selected Works of Liu Tungsheng*, edited by Z. An, pp. 192–202, Science Press, Beijing.

Liu, T., Z. Guo, J. Liu, J. Han, Z. Ding, Z. Gu, and N. Wu (1995), Variation of eastern Asian monsoon over the last 140,000 years, *Bull. Soc. Geol. Fr.*, *166*, 221–229.

McLennan, S. (1989), Rare earth elements in sedimentary rocks: Influence of provenance and sedimentary processes, in *Geochemistry and Mineralogy of Rare Earth Elements*, edited by B. R. Lipin and G. A. McKay, pp. 169–200, Mineral. Soc. of Am., Washington, D. C.

McLennan, S. (1993), Weathering and global denudation, *J. Geol.*, *101*, 295–303.

McLennan, S. (2001), Relationships between the trace element composition of sedimentary rocks and upper continental crust, *Geochem. Geophys. Geosyst.*, *2*(4), 1021, doi:10.1029/2000GC000109.

Nesbitt, H. (1979), Mobility and fractionation of rare earth elements during weathering of a granodiorite, *Nature*, *279*, 206–210, doi:10.1038/279206a0.

Nesbitt, H., and G. Markovics (1997), Weathering of granodioritic crust, long-term storage of elements in weathering profiles and petrogenesis of siliciclastic sediments, *Geochim. Cosmochim. Acta*, *16*, 1653–1670.

Nesbitt, H., and G. Young (1982), Early Proterozoic climates and plate motions inferred from major element chemistry of lutites, *Nature*, *299*, 715–717, doi:10.1038/299715a0.

Nesbitt, H., G. Markovics, and R. Price (1980), Chemical processes affecting alkalis and alkaline earths during continental weathering, *Geochim. Cosmochim. Acta*, *44*, 1659–1666, doi:10.1016/0016-7037(80)90218-5.

Nesbitt, H., G. Young, S. McLennan, and R. Keays (1996), Effects of chemical weathering and sorting on the petrogenesis of siliclastic sediments with implications for provenance studies, *J. Geol.*, *104*, 525–542.

Penfield, S. (1894), On some methods for the determination of water, *Am. J. Sci.*, *48*, 30–37.

Peng, S., and Z. Guo (2001), Geochemical indicator of original eolian grain size and the implications on winter monsoon evolution, *Sci. China, Ser. D*, *44*, suppl., 261–266.

Qiao, Y., Z. Guo, Q. Hao, Q. Yin, B. Yuan, and T. Liu (2006), Grain-size features of a Miocene loess-soil sequence at Qin'an: Implications on its origin, *Sci. China, Ser. D*, *49*, 731–738.

Sun, D., Z. An, J. Shaw, J. Bloemendal, and Y. Sun (1998), Magnetostratigraphy and paleoclimatic significance of Late Tertiary eolian sequence in the Chinese Loess Plateau, *Geophys. J. Int.*, *134*, 207–212, doi:10.1046/j.1365-246x.1998.00553.x.

Sun, X., and P. Wang (2005), How old is the Asian monsoon system?—Palaeobotanical records from China, *Palaeogeogr. Palaeoclimatol. Palaeoecol.*, *222*, 181–222, doi:10.1016/j.palaeo.2005.03.005.

Taylor, S., and S. McLennan (1985), *The Continental Crust: Its Composition and Evolution*, Blackwell, Oxford, U. K.

Taylor, S., S. McLennan, and M. Mcculloch (1983), Geochemistry of loess, continental crustal composition and crustal model ages, *Geochim. Cosmochim. Acta*, *47*, 1897–1905, doi:10.1016/0016-7037(83)90206-5.

Wen, Q. (1989), *Geochemistry of the Chinese Loess* (in Chinese), Science Press, Beijing.

Zachos, J., M. Pagani, L. Sloan, E. Thomas, and K. Billups (2001), Trends, rhythms, and aberrations in global climate 65 Ma to present, *Science*, *292*, 686–693, doi:10.1126/science.1059412.

Zhang, Z., and Z. Guo (2005), Spatial character reconstruction of different periods in Oligocene and Miocene (in Chinese with English abstract), *Quat. Sci.*, *25*, 523–530.